Title: Altered whole-brain connectivity in albinism

Abbreviated Title: Brain connectivity in albinism

Authors:

Thomas Welton (msxtw3@nottingham.ac.uk) [1]

Sarim Ather (sm326@leicester.ac.uk) [1, 2]

Frank A Proudlock (fap1@leicester.ac.uk) [2]

Irene Gottlob (ig15@leicester.ac.uk) [2]

Robert A Dineen (rob.dineen@nottingham.ac.uk) [1]

Affiliations:

[1] Radiological Sciences, Division of Clinical Neuroscience, University of Nottingham. Room W/B 1441, Queen's Medical Centre, Derby Road, Nottingham, NG7 2UH, United Kingdom.

[2] Ulverscroft Eye Unit, Ophthalmology, University of Leicester. Knighton Street Offices, Leicester Royal Infirmary, Leicester, LE2 7LX, United Kingdom.

Address Correspondence to:

Dr Rob Dineen, Room W/B 1441, Queen's Medical Centre, Derby Road, Nottingham, NG7 2UH, United Kingdom. Tel: +44 0(115) 823 1173. Fax: +44 (0)115 823 1180. E-mail: rob.dineen@nottingham.ac.uk.

Keywords: Albinism, Oculocutaneous; Diffusion Tensor Imaging; Functional Magnetic Resonance Imaging; Models, Biological; Neuronal Plasticity; Vision Disorders; Visual Cortex.

Abstract

Albinism is a group of congenital disorders of the melanin synthesis pathway. Multiple ocular, white matter and cortical abnormalities occur in albinism, including a greater decussation of nerve fibres at the optic chiasm, foveal hypoplasia and nystagmus. Despite this, visual perception is largely preserved. We proposed that this may be attributable to reorganisation among cerebral networks, including an increased interhemispheric connectivity of the primary visual areas.

We applied a graph-theoretic model to explore brain connectivity networks derived from resting-state functional and diffusion-tensor magnetic resonance imaging data in 23 people with albinism and 20 controls. We tested for group differences in connectivity between primary visual areas and in summary network organisation descriptors. We supplemented our main findings with analyses of control regions, brain volumes and white matter microstructure.

We found significant functional interhemispheric hyperconnectivity of the primary visual areas in the albinism group ($p=0.012$). Tests of interhemispheric connectivity based on the diffusion-tensor data showed no significant group difference ($p=0.713$). Second, we found that a range of functional whole-brain network metrics were abnormal in people with albinism, including the clustering coefficient ($p=0.005$), although this may have been driven partly by overall differences in connectivity, rather than reorganisation.

Based on our results, we suggest that changes occur in albinism at the whole-brain level, and not just within the visual processing pathways. We propose that our findings may reflect compensatory adaptations to increased chiasmic decussation, foveal hypoplasia and nystagmus.

Introduction

Albinism is a group of congenital disorders characterised by impairment of the melanin synthesis pathway. The condition is associated with a variety of ocular abnormalities including iris transillumination (Sheth et al. 2013), high refractive errors (Wang et al. 2010a), foveal maldevelopment (Mohammad et al. 2011) and optic nerve head abnormalities (Mohammad et al. 2015). In addition to ocular changes, the retro-ocular visual pathway is also affected: MRI studies have shown smaller optic nerves, tracts and chiasm in people with albinism (Schmitz et al. 2003). A particular hallmark of the disease is an increased decussation of fibres at the optic chiasm (Hoffmann et al. 2005, Von Dem Hagen et al. 2007). Alongside these white matter abnormalities, alterations in cortical architecture have also been reported. These include a shortened calcarine sulcus, reduced grey matter volume at the occipital pole, an increased cortical thickness and reduced occipital lobe gyrification, which all point to structural plasticity at the cortical level (Bridge et al. 2014).

Previous functional imaging and visual evoked potential studies (VEP) have demonstrated altered cortical activity in the primary visual (V1) region in relation to the anterior visual structural changes in albinism, showing visual cortex activation predominantly contralateral to the stimulated eye in patients (Morland et al. 2002, Hoffmann et al. 2003, Schmitz et al. 2004, von dem Hagen et al. 2008, Wolynski et al. 2010, Bridge et al. 2014). Given the range of abnormalities in albinism, however, visual perception remains relatively intact. One explanation for this may be that correction for the abnormal cortical representation occurs at later processing stages: Kaule et al. (2014) found that more specialised downstream visual areas also exhibited an atypical contralateral representation, and drew the conclusion that

cortico-cortical connections therefore follow a normal configuration. However, alterations in whole-brain structural and functional connectivity beyond the visual processing pathways have not been examined.

One way of studying brain connectivity involves the application of network science to brain imaging data (Bullmore and Sporns 2009, Park and Friston 2013). Network science is founded in graph theory, which is a system for mathematically describing the interrelationships between groups of objects. Under the graph-theoretic model, brain regions are represented by *nodes* in a graph and the connections between them are represented by *edges*, which may be based on any measure of connectivity; for example, functional MRI- (fMRI), EEG- or magnetoencephalography-derived functional connectivity or diffusion tensor imaging (DTI) tractography streamline counts. Given a graph of the brain, summary metrics can be calculated to describe its organisational structure and to allow statistical comparisons to be made (Rubinov and Sporns 2010b).

We propose that one possible mechanism by which visual perception remains relatively intact may be an increased interhemispheric connectivity of visual areas in compensation for the increased crossing of fibres at the chiasm. The rationale for this claim is that, if the proportion of decussating fibres at the chiasm is abnormally great, yet visual perception is mostly preserved, then the signals from the right visual field may cross back to the right visual processing areas (and vice-versa) at some point “downstream”; the most direct route being between the primary visual cortices via the splenium of the corpus callosum. Alternatively, it may be the case that cortical reorganisation occurs more locally within each hemisphere in such a way that copes with an abnormally great representation of the contralateral visual field.

In this study we examine whether structural and functional cerebral reorganisations in people with albinism are detectable as differences in brain connectivity and network organisation metrics when compared to controls. In particular, we test two hypotheses: (1) that albinism will be associated with increased interhemispheric connectivity of the V1 region compared to controls, and (2) that the organisational properties of the functional and structural whole-brain networks may be different in people with albinism compared to controls.

Materials and Methods

Participants

Twenty-three people with albinism (6 females; mean age 34±13.6, range 18-64) were recruited through the neuro-ophthalmology outpatient clinic at the Leicester Royal Infirmary. Twenty age-, gender- and ethnicity-matched volunteers were recruited for the control group (6 females; mean age 31.9±10.6, range 21-54) from within the students and faculty at the University of Leicester as well as healthy spouses of albinism patients. Controls were included in the study if they had no history of eye disease and had a best-corrected visual acuity (VA) of better than 0.0 logMAR in each eye. The study was approved by the local research and ethics board and prior to participating in the study, informed consent was sought from all volunteers.

Data Acquisition

Each volunteer underwent a detailed clinical examination which included assessment of best-corrected VA, visual fields, pupil reactions, ocular movements, slit lamp examination and dilated fundus examination. VEP testing was carried out in

accordance with the international society for clinical electrophysiology of vision standards (Odom et al. 2010) and the degree of asymmetry was quantified by means of an intra-hemispheric asymmetry index described by Apkarian et al. (1983). An EyeLink II pupil tracker (SR Research, Osgoode, Canada) was used to record horizontal and vertical eye movements in all patients. During the recordings, the patients were asked to fixate on a target which shifted from 30° to the left to 30° to the right in 3° steps every 7 seconds. Spike2 software (Cambridge Electronic Design, Cambridge, UK) scripts were used to calibrate the recording offline and to calculate the amplitude, frequency and intensity (amplitude × frequency) of nystagmus at each 3° interval and then averaged across all gaze positions for final analysis.

Subjects underwent an MRI scan at 3T (Philips Achieva, Eindhoven, NL), including T1-weighted (axial MPRAGE, TR=7.53 ms, TE=2.22 ms, flip angle=8°, matrix size 320 x 320, field of view=256 x 256, 0.8mm isotropic voxels, SENSE factor=1.7, 184 contiguous slices), resting-state fMRI with eyes closed (axial echo-planar imaging acquisition, TE=36ms, TR=2100ms, matrix size 80 x 80, 35 contiguous slices, 140 volumes, 3mm isotropic voxels, 4.9 minutes scan time) and DTI (axial diffusion-weighted echo-planar imaging, six *b*=0 volumes averaged during acquisition and 61 directional diffusion weighted images with b=1000 s/mm^2, TE=67ms, TR=8270ms, sense factor 3, matrix size 240 x 240, 52 contiguous slices, 1.8 x 1.8 x 1.8 mm voxels interpolated to 0.9 x 0.9 x 1.8mm) acquisitions.

Image Processing

FreeSurfer (version 5.3.0; http://surfer.nmr.mgh.harvard.edu/) was used to perform anatomical surface-based parcellation of the high-resolution MPRAGE images

(Fischl 2012). First, non-brain tissue was removed, and then a transformation to Talairach space was applied. Images were then parcellated into 164 cortical and subcortical regions-of-interest (ROIs; listed in Table S-III) based on the Destrieux atlas of gyral and sulcal structures (Destrieux et al. 2010). FreeSurfer was also used to reconstruct the cortical surface and to estimate the thickness and volume of each ROI.

FMRI data underwent the following processing steps using fMRIB's Software Library (FSL; version 5.0.7; http://www.ndcn.ox.ac.uk/divisions/fmrib/; Jenkinson et al. (2012)). First, the first 2 volumes of each dataset were removed to allow for steady-state imaging to be reached. Head motion was corrected for by affine registration to the middle volume using MCFLIRT and any datasets having excessive motion artefacts were removed (cumulative rotation or translation >3° or >4 mm over the 4.9-minute scan). Non-brain structures were removed using the FSL brain extraction tool (BET). Spatial smoothing was not used, to avoid introducing local correlations between adjacent ROIs. Since the FreeSurfer-generated ROIs were in Talairach space, the FreeSurfer brain images were registered to the fMRI datasets using FSL FLIRT and the resulting transformation matrix applied to the ROIs in order for them to be mapped onto fMRI space. After extracting the mean BOLD timeseries across all voxels in each ROI, low-frequency drift was corrected for by removing the linear trend from the data. Then, the following nuisance signals were regressed: six motion parameters (three translation and three rotation), the mean signal from the ventricles and the mean signal from the white matter. This number of nuisance regressors was shown to be an optimal balance between denoising and signal loss for datasets of a similar number of timepoints (Bright and Murphy 2015). Finally, the degree of functional connectivity between each pair of ROIs was quantified by a Pearson

correlation coefficient. These coefficients were used to construct a symmetric matrix of size 164 × 164, with each element representing the degree of functional connectivity between two ROIs.

DTI data were processed using fMRIB's Diffusion Toolbox (FDT) in FSL. First, artefacts induced by head motion and eddy currents were corrected by registering all image volumes to the average *b*=0 image with an affine transformation. Non-brain structures were removed with BET, and then diffusion parameters were estimated using BEDPOSTX (Bayesian Estimation of Diffusion Parameters Obtained using Sampling Techniques; (Behrens et al. 2007)). ROIs were moved to DTI space by registering the FreeSurfer brain image to the average *b*=0 image with an affine transformation in FLIRT and applying the transformation matrix to the ROIs. Probabilistic fibre tracking was performed using the streamline tractography algorithm, PROBTRACKX2. The algorithm propagates streamlines from each voxel in a given seed mask along the path with the largest principal axis of each voxel's diffusion tensor until some termination criteria are met (in this case, when the streamline reached the voxels in a termination mask). By applying this process to every pair of ROIs, a matrix of size 164 × 164, was constructed where each element represents the number of streamlines between a pair of ROIs. Because the number of streamlines between the seed and terminal ROI could vary depending on direction, it was measured twice between each ROI pair; once in each direction (i.e. the connectivity matrices were asymmetric). These streamline counts were then combined and scaled by the size of the two ROIs (as in Cheng et al. (2012), Owen et al. (2013), Buchanan et al. (2014)) using the following formula, to obtain a measure of streamline density:

$$a_{ij} = \frac{s_{ij} + s_{ji}}{m_i + m_j}$$

where a_{ij} is the corrected summary streamline count, s_{ij} and s_{ji} are streamline counts in each direction between ROIs i and j, and m_i and m_j are voxel counts in each ROI.

Primary Visual Cortex Connectivity

Shapiro-Wilk tests and visual inspection of quantile-quantile plots determined whether or not each variable followed a normal distribution and t-tests or Mann-Whitney U tests were used as appropriate.

We first wanted to test how strongly-connected the V1 regions of each hemisphere were to each other in each group. To achieve this, the functional connectivity and streamline density measurements between the calcarine sulcus FreeSurfer ROI (FreeSurfer IDs 11145 and 12145), in which the V1 region is located (Wandell 1995, Wandell et al. 2007), in each hemisphere were tabulated and tested for equality.

To assess whether any identified group difference in V1-V1 connectivity was due to an overall higher connectivity of the V1 to all regions, we then compared the V1 connectivity to every other contralateral ROI between groups.

Since streamline density may be problematic as a measure of connectivity strength (Jones et al. 2013), we performed additional tests of fractional anisotropy (FA; a general measure of microstructural integrity) and mean diffusivity (MD; a measure of membrane density) in a 12-voxel ROI in the splenial corpus callosum of each subject and compared the mean scores between groups. These ROIs were defined by identifying the two central sagittal slices and placing a 3 × 2 ROI in each, in the

centre of the splenium. We also tested for group differences in whole-brain FA, as a global effect may have confounded our connectivity findings in individual regions.

As a further control, we tested the interhemispheric connectivity of a region comprising the frontomarginal gyrus and the frontal pole (connected by the genu of the corpus callosum), and of the medial temporal cortex (connected by the splenium of the corpus callosum). The frontal region was defined by the frontal pole and frontomarginal gyrus FreeSurfer labels and was chosen for its similar size and proximity to the corpus callosum as the V1 area. The medial temporal cortex region was defined as the parahippocampal gyrus FreeSurfer label. These analyses were performed for both functional and streamline density data.

To test whether any difference in V1 connectivity was due to between-subject differences in cortical thickness we used the cortical thickness measurements from the calcarine sulcus FreeSurfer ROI to perform two correlation tests, between either the functional connectivity or streamline density between left and right primary visual cortices and the average cortical thickness between both hemispheres of the calcarine sulcus region.

Finally, we also tested the interhemispheric connectivity of the anterior and posterior regions of V1 separately. We suspected that stronger between-group differences might be found in the posterior V1, which represents the central visual field, in which the abnormal visual representation is most dominant, as opposed to the anterior V1, representing the peripheral visual field. The ideal way to split the V1 ROI into anterior and posterior portions would have been to measure each voxel's BOLD modulation to stimulation at varying locations in the visual field in a per-subject fashion (Wandell et al. 2007), but as we did not have this data available we opted to simply split the

region halfway along the anterior/posterior axis. Based on previous neuroanatomic research (Yu et al. 2014, Li et al. 2015), we believe this approach would capture the majority of an effect. We then applied the same method as we had previously to measure the functional connectivity and streamline density between left and right anterior V1 ROIs, and left and right posterior V1 ROIs.

Whole-Brain Network Properties

To explore group differences in whole brain structural and functional networks, we constructed the functional connectivity and streamline density matrices as graphs, allowing calculation of summary network metrics (Figure 1). The two types of association matrix contained all the information necessary to describe weighted graphs, where each ROI is modelled by a node and each connectivity value is modelled by a weighted edge. To the functional connectivity matrices, we applied Fisher's Z transformation**,** and to the SD matrices we re-scaled the weights such that they were between 0 and 1. In order for spurious connections to be removed and the strong ones retained, a minimum density threshold was applied to each graph (a graph's density is the ratio of the existing edges to possible edges). Further, to avoid performing multiple comparisons and having to select a single arbitrary threshold, a range of density thresholds were applied, rather than a single threshold, and the integral over this range taken as a summary metric score, as in Hosseini et al. (2012). We thresholded the graphs over a density range of 0.1 – 0.4, in steps of 0.02. This range represents a compromise between being too dense to show small-world properties and being so sparse that fragmentation begins to occur (Bassett and Bullmore 2006, Fornito et al. 2010). The density threshold was implemented by checking the graph density and incrementing a connection strength threshold repeatedly, until the target density is reached. The following whole-brain summary

graph metrics were calculated from the weighted graphs in MATLAB using the Brain Connectivity Toolbox (BCT; for detailed descriptions of each, see Rubinov and Sporns (2010a)):

(1) Clustering coefficient of a single node is the proportion of its neighbours (connected nodes) that are connected to each other. It is given by:

$$C_i = \frac{2N}{k_i(k_i - 1)}$$

where k_i is the degree of node i (the number of edges connected to it) and N is the number of connections existing between neighbouring nodes. The global clustering coefficient is the average of clustering coefficients across all nodes in the network.

(2) Characteristic path length. Given two nodes, i and j, the shortest path between them is the path with the greatest weight. The characteristic path length L is the average of all shortest paths across a whole network. In this instance, distances were calculated using the inverse of the association matrix to account for the fact that higher correlations or streamline densities should indicate shorter paths, not longer paths.

(3) Small-worldness. Introduced by Watts and Strogatz (1998), small-worldness is the property of being highly clustered and being able to reach any node in a small number of steps from any other. We quantified small-worldness with the equation:

$$\omega = \frac{\left(\frac{C}{C_{random}}\right)}{\left(\frac{L}{L_{random}}\right)}$$

Where C_{random} and L_{random} are the mean clustering coefficient and characteristic path length of 20 randomly-generated networks of the same number of nodes and edges as our network.

(4) Assortativity refers to a node's tendency to connect with nodes of a similar degree. It is given by the Pearson correlation coefficient of the degree of each pair of connected nodes (Newman 2002).

(5) Modularity. Newman's spectral optimisation method (Newman 2006) was used to divide the graph into subsets of nodes that connect more within themselves than they do to the rest of the graph (called modules). The strength of this division was then used as a summary measure of modularity, defined as the fraction of edges in the selected modules minus the fraction of edges in the modules if the edges in the network were assigned randomly.

These metrics were selected based on their reproducibility and frequency of appearance in the literature (Welton et al. 2014).

All graph metric results were then compared to a value which was the average of that metric across 1000 randomly-generated networks which preserved degree sequence. The final summary scores for each subject were the ratio of their metric values to the values from the 1000 random networks. This was performed using custom scripts and the BCT in MATLAB. For presentation in the figures only, these scores were standardised by subtracting the mean of the group and then dividing by the standard deviation of the group.

We repeated the graph analysis in two subsets of nodes: one restricted to 44 nodes known to have some relevance to visual processing and one in 120 nodes excluding

those visual regions (Table S-III). This would indicate whether the whole-brain network changes were driven by alterations to visual or non-visual areas of the brain.

Again, we used Shapiro-Wilk tests and quantile-quantile plots to determine whether or not the graph metrics followed normal distributions for either group. Between-group differences in the summary metrics were calculated with the appropriate statistical test.

Relation to Clinical Measures

Within the albinism group, Pearson correlations of average VA, VEP asymmetry, age and sex to average functional connectivity and streamline density between primary visual areas, as well as the graph metrics were calculated. VA and VEP measurements were not available in the control group. Finally, we tested the effect of nystagmus amplitude, frequency and intensity on the interhemispheric connectivity and graph metrics with tests for correlation.

We applied the Benjamini-Hochberg procedure (Benjamini and Hochberg 1995) to correct for the false discovery rate (FDR).

Results

Sample Characteristics

The difference in ages between groups was not statistically significant ($t = 0.85$, $p = 0.41$). In the albinism group, the median VEP asymmetry index was 1.48 (IQR 1.29-1.64) and the median LogMAR VA was 0.50 (IQR 0.27-0.60). These scores indicate that, while the albinism group did demonstrate a degree of asymmetry seen previously (Apkarian and Shallo-Hoffmann 1991), their visual acuity was mostly classed as either not impaired or only mildly impaired. Good quality MPRAGE and

DTI scans were acquired from all volunteers but one fMRI dataset had to be excluded from the albinism group due to motion artefacts, thus reducing the sample size for fMRI analysis to 42.

Total brain volume may have been a possible confounding factor in our measurements of functional connectivity and streamline density. However, brain volumes (including cerebral white and grey matter, and not including the ventricles, other CSF, cerebellum or the brain stem) were not significantly different between groups ($t = 0.548$, $p = 0.587$), nor were volumes of the calcarine sulcus grey matter in either hemisphere (left: $t = -0.124$, $p = 0.902$; right: $t = -0.523$, $p = 0.604$).

Head motion is another known confound of connectivity analyses. The mean relative displacements of the albinism and control groups were 0.15 (±0.07) mm and 0.11 (±0.04) mm respectively. A t-test of the values showed no significant between-group difference ($t = -1.716$, $p = 0.093$). Thus the likelihood of any groupwise differences in connectivity-based metrics being related to subject motion in the scanner is low.

Primary Visual Cortex Connectivity

Figure 2 and Table I show the results of the calcarine sulcus connectivity analysis. Mann-Whitney U tests showed that the albinism group had a significantly greater interhemispheric functional connectivity of the primary visual cortex region compared to controls (median albinism correlation coefficient = 0.74, median control correlation coefficient = 0.61, $U = 164$, $p = 0.012$). These values are consistent with those reported in the literature (Butt et al. 2013, Donner et al. 2013, Raemaekers et al. 2014). For streamline density, there was no significant difference (albinism median = 10.64, control median = 8.78, $U = 174$, $p = 0.713$). In the tests of connectivity in the anterior and posterior subregions of the V1 (Table I), we found, as expected,

significant group differences in functional connectivity which were slightly greater in the posterior region ($U = 160$, $p = 0.010$) compared to the anterior region ($U = 178$, $p = 0.030$), but no significant group differences in the structural data ($U = 152$, $p = 0.322$; $U = 146$, $p = 0.246$).

To test whether this was reflecting an overall higher global connectivity of the calcarine sulcus region in albinism, or whether it was specifically more strongly connected only to the contralateral calcarine sulcus, we compared, using t-tests, the connectivity values of the calcarine sulci to all other regions between groups. To do this, we measured the mean connectivity across the whole of each group (for both functional connectivity and streamline density) between the calcarine sulcus and every other region in the atlas. We found that the calcarine sulcus did not tend to be more strongly connected functionally in either group ($t = 1.569$, $p = 0.117$). For the streamline density data, there was also no significant difference ($t = -1.322$, $p = 0.186$). Thus, the between-group differences in interhemispheric connectivity of the calcarine sulcus were likely not caused by a greater average connectivity of the calcarine sulcus in albinism patients.

T-tests of FA and MD in the splenial corpus callosum showed no significant between-group differences (FA: albinism mean = 0.652, control mean = 0.657, $t = 0.109$, $p = 0.913$; MD: albinism mean = 0.001, control mean = 0.001, $t = 0.732$, $p = 0.468$). There were also no significant effects for global FA or MD (FA: albinism mean = 0.257, control mean = 0.255, $t = -0.389$, $p = 0.699$; MD: albinism mean = 0.001, control mean = 0.001, $t = 0.203$, $p = 0.840$). These results suggest that there are little or no microstructural abnormalities in the V1-V1 pathway in albinism.

In our tests of interhemispheric connectivity in the control regions, we found that there were no significant differences between groups for the functional data (frontal: $t = -1.334$, $p = 0.190$; medial temporal: $t = -1.472$, $p = 0.149$) or the structural data (frontal: $t = -0.474$, $p = 0.638$; medial temporal: $t = -0.857$, $p = 0.397$). These results suggest that our finding of increased interhemispheric connectivity of V1 in people with albinism is not an artefact of a whole-brain effect.

(Fig. 2 here.)

(Table I here.)

In the correlations of functional connectivity and streamline density with cortical thickness, there was no significant correlation for functional connectivity ($r = -0.073$, $p = 0.648$) or for streamline density ($r = 0.135$, $p = 0.413$). This indicates that cortical thickness was unlikely to have been a confounding factor.

Whole-Brain Network Properties

Tables II and III, and Figure 3 show the results of the tests for between-group differences in graph metric integrals. In the whole-brain networks derived from fMRI data, the clustering coefficient and small-worldness metric integrals were significantly higher in the albinism group. The characteristic path length and modularity metric integrals did not reach significance when accounting for multiple comparisons. The assortativity metric did not show any association to group membership. In the whole-brain networks derived from DTI data, none of the metrics showed significant differences between the two groups (Table III).

To test whether the differences in whole-brain metrics in the albinism group were mostly driven by the differences in connectivity of the primary visual area, we tested

for correlation between each subject's interhemispheric calcarine sulcus connectivity and their whole-brain metric scores and found that the effect was significant for only the clustering coefficient and small-worldness metrics in the functional connectivity dataset (Tables S-I & S-II). These results indicate that one contributing factor to alterations in subjects' graph metric scores was likely to be the increased interhemispheric connectivity of the V1 region.

The results of the analysis of visual-only and non-visual-only networks are given in Tables S-IV – S-VII. We find that the only significant differences between the groups were in the non-visual networks based on fMRI data. Specifically, the clustering coefficient ($t = -3.530$, $p = 0.001$), characteristic path length ($t = -2.876$, $p = 0.006$) and small-worldness ($t = -3.762$, $p = 0.001$) metrics showed significant differences between groups. The assortativity ($t = -0.856$, $p = 0.397$) and modularity ($t = -1.701$, $p = 0.097$) metrics were not significantly different, nor were any of the metrics from the non-visual DTI networks or visual-only networks.

Because our results pointed to a global change in brain connectivity, we calculated the total sum of the connectivity matrix for both functional connectivity and streamline density data. We found that the sum of the functional matrices was greater on average for people with albinism, but not significantly so ($t = -1.695$, $p = 0.097$). For streamline density matrices, the control group had significantly greater matrix sums ($t = 2.229$, $p = 0.033$). This suggests that the overall level of conenctivity in general may have also been a factor in our main graph results.

Within the albinism group, neither VA, VEP, age nor sex correlated with any of the graph metrics for either functional or structural networks. We found that nystagmus intensity did not significantly correlate with either interhemispheric functional

connectivity ($r = 0.128$, $p = 0.591$), streamline density ($r = 0.141$, $p = 0.589$), or any of the graph metrics.

(Table II here.)

(Table III here.)

(Fig. 3 here.)

Discussion

This study investigated the functional and structural architecture of brain networks and connectivity of the visual cortex in people with albinism relative to healthy controls. The results of our analysis of brain connectivity based on functional and diffusion-tensor MRI support our hypothesis that greater interhemispheric connectivity of the primary visual cortex may exist in albinism compared to controls. We also explored functional and structural brain network organisation and found that functional networks were significantly altered in albinism and structural networks were not. However, our results should be interpreted with care for several reasons discussed here. Ours is the first study, to our knowledge, that has examined the brains of people with albinism using the graph-theoretic model. Therefore, our findings could provide novel insights into how normal visual perception is largely preserved despite extensive abnormal development of the visual system, and into brain plasticity in general.

Hyperconnectivity of the Primary Visual Cortex

Firstly, we found that the two primary visual cortices were functionally hyperconnected in the albinism group. The between-group difference in functional connectivity suggests greater-than-normal connection strength between primary

visual cortices in opposite hemispheres. This finding may reflect a compensatory adaptation in response to abnormal visual input. Recent studies show the brain's capacity for extensive plasticity in both acute injury; for example, spinal cord injury (Ding et al. 2005), stroke (Liepert et al. 2000) and traumatic brain injury (TBI) (Sidaros et al. 2008); and in developmental or congenital disorders affecting the CNS, like deafness (Kral and Sharma 2012). In albinism, the brain must adapt to a number of abnormalities including reduced foveal input caused by foveal hypoplasia, constant retinal motion associated with nystagmus and miswired cortical inputs due to chiasmal misrouting.

Studies have shown increased V1 cortical thickness in albinism compared to controls (Bridge et al. 2014), in blindness (Jiang et al. 2009) and in anophthalmia (Bridge et al. 2009). One study showed that cortical thickness was negatively correlated with functional activation of the occipital lobe in the early blind during sound localisation and pitch identification tasks (Anurova et al. 2014). It is therefore plausible that cortical thickness had an effect on our connectivity measurements. However, our correlation analysis showed that the variance in functional connectivity or streamline density was not explained by differences in cortical thickness. This suggests that any between-group differences in functional connectivity or streamline density were more likely due to true differences in strength of connectivity, rather than differences in cortical thickness of the calcarine sulcus region or overall brain size, but this may also be an effect of our having corrected streamline count for ROI size.

We found no significant group difference in calcarine sulcus volume. One possible explanation for this is that, because the abnormality in albinism at the fovea, corresponding to the central visual field, relates most to changes in the posterior calcarine sulcus, and because our ROI covered a larger area, that any significant

effect was lost. This is supported by a previous study which found reduced volume posteriorly in the calcarine sulcus i.e. at the occipital pole (von dem Hagen et al. 2005). That the V1 region would have an increased thickness in albinism but also a decreased or unchanged volume may be explained by a reduced cortical gyrification and length (Bridge et al. 2014).

There are several possible reasons why there was no group difference in the streamline density outcomes. First, there are issues in the interpretation of tractography streamline counts: even where the true number of axonal projections within a bundle is uniform, the length, curvature and branching may affect the number of reconstructed streamlines (Jones et al. 2013). Hence, our streamline data should not be interpreted in terms of real fibres; our use of the term ‘streamline density’ rather than ‘fibre count’ was deliberate in order to reflect this. It is also plausible that, while the brain is forced to adapt to abnormal visual development, the degree of adaptation is not enough that it confers measurable structural changes, or even any structural changes at all.

Differences in Brain Network Organisation

The graph-theoretic model of brain connectivity has shown in recent years that the organisational properties of macroscopic whole-brain networks are related to certain disease states. For example, in a study of 203 people with schizophrenia and 259 controls, it was found that brain network organisation in the schizophrenia group was abnormal by comparison, with significantly reduced hierarchy scores, increased connection distances and the loss of hubs in the frontal cortex (Bassett et al. 2008). There have also been positive results in other diseases including multiple sclerosis (Rocca et al. 2014), Alzheimer’s disease (He et al. 2008), attention deficit

hyperactivity disorder (ADHD) (Wang et al. 2009), autism (Rudie et al. 2013) and depression (Leistedt et al. 2009). For reviews, see Bassett and Bullmore (2009), Guye et al. (2010), Wang et al. (2010b), and Menon (2011).

Our analysis of brain network properties also demonstrated functional changes associated with albinism. Two of the functional connectivity-based metrics were significantly different (clustering coefficient and small-worldness), and two more (characteristic path length and modularity) showed strong but non-significant differences after multiple comparison correction, while none of the metrics based on streamline density measurements were significantly different between groups. Our control analyses indicated that overall differences in connectivity may have been a determining factor in these results, so they should be interpreted carefully. The small-world attribute is thought to be characterised by an optimal balance of both local and global integration, leading to efficient information transfer. Despite deficits in other network metrics, small-worldness is often conserved or increased, for example in Alzheimer's disease (He et al. 2008), epilepsy (Liao et al. 2010), ADHD (Wang et al. 2009), autism (Barttfeld et al. 2011), schizophrenia (Lynall et al. 2010), TBI (Nakamura et al. 2009, Kou and Iraji 2014) and sleep deprivation (Liu et al. 2014). Liu et al. (2014) suggested that elevated small-worldness may represent "a possible compensatory adaptation of the human brain." The clustering coefficient describes the connectedness of a node's neighbours to give a measure of local integration. A higher clustering coefficient compared to controls has been reported in studies of cognitive dysfunction in low-grade glioma patients (Bosma et al. 2009), epilepsy (Soltesz and Staley 2011), Alzheimer disease (He et al. 2008, Mccarthy et al. 2014), TBI (Castellanos et al. 2011), small-vessel disease (Kim et al. 2015), obsessive compulsive disorder (Zhong et al. 2014) and chronic disorders of

consciousness in patients recovered from coma (Crone et al. 2014). While these studies do show that brain network properties are often altered in disease, authors can only speculate as to the specific meaning of those alterations. Similarly, the implications of these changes for albinism are unknown; only that they suggest widespread reorganisation and may give a clue as to the pattern of connectivity differences that are present.

Our graph analyses of regions involved in visual processing and regions not involved suggests that, although V1-V1 connectivity was increased in albinism, this was not sufficient to confer significant changes to the overall organisation of the visual networks. On the other hand, we found that the graphs formed from only non-visual regions were significantly different between groups. One study of brain networks and V1 connectivity in the congenitally blind had similar findings and proposed the following explanation: “while the internal structural organization of the visual cortex was strikingly similar, the blind exhibited profound differences in functional connectivity to other (non-visual) brain regions as compared to the sighted” (Striem-Amit et al. 2015).

Previous functional imaging studies of albinism have maintained focus on the visual cortical areas (Morland et al. 2002, Hoffmann et al. 2003, Schmitz et al. 2004, von dem Hagen et al. 2008, Wolynski et al. 2010, Bridge et al. 2014). Hoffmann and Dumoulin (2015) reviewed cortical plasticity in congenital visual pathway abnormalities, and concluded that “the organisation of subcortical and higher cortical projection targets in the visual pathway … will be rewarding targets for research”. Ours is the first study which suggests that albinism is associated with not only changes to visual brain areas, as traditionally thought, but also with wider changes to other brain areas.

Study Limitations

Our study had multiple limitations. Firstly, while the reliability of graph-based summary metrics has recently been shown to be excellent under the right circumstances, their correct interpretation in biological and clinical contexts is still largely unknown (Rubinov and Sporns 2010a, Welton et al. 2014). This has meant that studies of summary graph metrics in the brain have difficulty forming strong hypotheses, have issues with multiple comparisons, and are necessarily exploratory in nature. Future work to alleviate this will develop theories about what the various metrics mean in terms of neurobiology, rather than in terms of graphs in the abstract sense.

Second, since nystagmus was present in all of the participants with albinism, it is feasible that some of the observed between-group differences were an artefact of involuntary eye movement rather than differences in functional connectivity. Our correlation analyses of nystagmus amplitude, intensity and frequency showed that this effect was probably small in our sample. The effect was likely to have been lessened by the fact that the fMRI scans were performed with eyes closed.

We were unable to control for subjects' level of education, which may have impacted our results, given that some of the controls were university faculty. No physiological data were gathered during the fMRI scan and, hence, while we did regress white matter and CSF signals (Hallquist et al. 2013), we could not fully account for this factor in our analysis and our data may have been affected by this source of noise. Finally, it has been shown that the reliability of fMRI connectivity estimates can be greatly improved by increasing the scan length up to 13 minutes. Our estimates may therefore be improved upon, since our scans lasted only 4.9 minutes.

Conclusions

Together, our findings indicate that the brains of people with albinism are functionally adapted to abnormal visual input but that the functional adaptations do not seem to be accompanied by white matter changes. Our findings may reflect a compensatory functional adaptation accounting for the increased decussation of the optic nerve fibres at the chiasm, foveal hypoplasia and nystagmus. Our results suggest that wider changes throughout the whole brain occur in albinism, rather than only in the visual processing pathways. We propose that these wider changes may be secondary to adaptation of the visual pathways, and may suggest a general propagation effect of functional adaptation throughout the brain.

Author Contributions: SM, FAP, IG and RAD designed and performed the experiment. TW and SM analysed the data with advice from FAP, IG and RAD. TW, SM, and RAD wrote the paper. All authors contributed to and commented on the manuscript.

Conflict of Interest: The authors declare no competing financial interests.

Acknowledgements: This work was supported by a research grant from the Medisearch Foundation. TW was supported by a studentship grant from the UK Multiple Sclerosis Society. The authors thank Dr Paul Morgan for developing the DTI protocol and Dr Yue Xing for discussions on the graph analysis.

References

Anurova I, Renier LA, De Volder AG, Carlson S, Rauschecker JP (2014) Relationship Between Cortical Thickness and Functional Activation in the Early Blind. Cereb Cortex (in press).

Apkarian P, Reits D, Spekreijse H, Van Dorp D (1983) A decisive electrophysiological test for human albinism. Electroencephalogr Clin Neurophysiol 55(5): 513-531.

Apkarian P, Shallo-Hoffmann J (1991) VEP projections in congenital nystagmus; VEP asymmetry in albinism: a comparison study. Invest Ophthalmol Vis Sci 32(9): 2653-2661.

Barttfeld P, Wicker B, Cukier S, Navarta S, Lew S, Sigman M (2011) A big-world network in ASD: dynamical connectivity analysis reflects a deficit in long-range connections and an excess of short-range connections. Neuropsychologia 49(2): 254-263.

Bassett DS, Bullmore E (2006) Small-world brain networks. The neuroscientist 12(6): 512-523.

Bassett DS, Bullmore E, Verchinski BA, Mattay VS, Weinberger DR, Meyer-Lindenberg A (2008) Hierarchical organization of human cortical networks in health and schizophrenia. J Neurosci 28(37): 9239-9248.

Bassett DS, Bullmore ET (2009) Human brain networks in health and disease. Curr Opin Neurol 22(4): 340-347.

Behrens TE, Berg HJ, Jbabdi S, Rushworth MF, Woolrich MW (2007) Probabilistic diffusion tractography with multiple fibre orientations: What can we gain? Neuroimage 34(1): 144-155.

Benjamini Y, Hochberg Y (1995) Controlling the False Discovery Rate: A Practical and Powerful Approach to Multiple Testing. Journal of the Royal Statistical Society. Series B (Methodological) 57(1): 289-300.

Bosma I, Reijneveld JC, Klein M, Douw L, van Dijk BW, Heimans JJ, Stam CJ (2009) Disturbed functional brain networks and neurocognitive function in low-grade glioma patients: a graph theoretical analysis of resting-state MEG. Nonlinear Biomed Phys 3(1): 9.

Bridge H, Cowey A, Ragge N, Watkins K (2009) Imaging studies in congenital anophthalmia reveal preservation of brain architecture in 'visual' cortex. Brain 132(Pt 12): 3467-3480.

Bridge H, von dem Hagen EA, Davies G, Chambers C, Gouws A, Hoffmann M, Morland AB (2014) Changes in brain morphology in albinism reflect reduced visual acuity. Cortex 56: 64-72.

Bright MG, Murphy K (2015) Is fMRI “noise” really noise? Resting state nuisance regressors remove variance with network structure. NeuroImage 114: 158-169.

Buchanan CR, Pernet CR, Gorgolewski KJ, Storkey AJ, Bastin ME (2014) Test-retest reliability of structural brain networks from diffusion MRI. Neuroimage 86: 231-243.

Bullmore E, Sporns O (2009) Complex brain networks: graph theoretical analysis of structural and functional systems. Nature Reviews Neuroscience 10(3): 186-198.

Butt OH, Benson NC, Datta R, Aguirre GK (2013) The fine-scale functional correlation of striate cortex in sighted and blind people. J Neurosci 33(41): 16209-16219.

Castellanos NP, Leyva I, Buldu JM, Bajo R, Paul N, Cuesta P, Ordonez VE, Pascua CL, Boccaletti S, Maestu F, del-Pozo F (2011) Principles of recovery from traumatic brain injury: reorganization of functional networks. Neuroimage 55(3): 1189-1199.

Cheng H, Wang Y, Sheng J, Kronenberger WG, Mathews VP, Hummer TA, Saykin AJ (2012) Characteristics and variability of structural networks derived from diffusion tensor imaging. Neuroimage 61(4): 1153-1164.

Crone JS, Soddu A, Höller Y, Vanhaudenhuyse A, Schurz M, Bergmann J, Schmid E, Trinka E, Laureys S, Kronbichler M (2014) Altered network properties of the fronto-parietal network and the thalamus in impaired consciousness. NeuroImage: Clinical 4(0): 240-248.

Destrieux C, Fischl B, Dale A, Halgren E (2010) Automatic parcellation of human cortical gyri and sulci using standard anatomical nomenclature. NeuroImage 53(1): 1-15.

Ding Y, Kastin AJ, Pan W (2005) Neural Plasticity After Spinal Cord Injury. Current pharmaceutical design 11(11): 1441-1450.

Donner TH, Sagi D, Bonneh YS, Heeger DJ (2013) Retinotopic patterns of correlated fluctuations in visual cortex reflect the dynamics of spontaneous perceptual suppression. J Neurosci 33(5): 2188-2198.

Fischl B (2012) FreeSurfer. Neuroimage 62(2): 774-781.

Fornito A, Zalesky A, Bullmore ET (2010) Network scaling effects in graph analytic studies of human resting-state FMRI data. Frontiers in systems neuroscience 4.

Guye M, Bettus G, Bartolomei F, Cozzone PJ (2010) Graph theoretical analysis of structural and functional connectivity MRI in normal and pathological brain networks. MAGMA 23(5-6): 409-421.

Hallquist MN, Hwang K, Luna B (2013) The nuisance of nuisance regression: spectral misspecification in a common approach to resting-state fMRI preprocessing reintroduces noise and obscures functional connectivity. Neuroimage 82: 208-225.

He Y, Chen Z, Evans A (2008) Structural insights into aberrant topological patterns of large-scale cortical networks in Alzheimer's disease. J Neurosci 28(18): 4756-4766.

Hoffmann MB, Dumoulin SO (2015) Congenital visual pathway abnormalities: a window onto cortical stability and plasticity. Trends in Neurosciences 38(1): 55-65.

Hoffmann MB, Lorenz B, Morland AB, Schmidtborn LC (2005) Misrouting of the optic nerves in albinism: estimation of the extent with visual evoked potentials. Investigative ophthalmology & visual science 46(10): 3892-3898.

Hoffmann MB, Tolhurst DJ, Moore AT, Morland AB (2003) Organization of the visual cortex in human albinism. The Journal of neuroscience 23(26): 8921-8930.

Hosseini SM, Hoeft F, Kesler SR (2012) GAT: a graph-theoretical analysis toolbox for analyzing between-group differences in large-scale structural and functional brain networks. PLoS One 7(7): e40709.

Jenkinson M, Beckmann CF, Behrens TE, Woolrich MW, Smith SM (2012) FSL. Neuroimage 62(2): 782-790.

Jiang J, Zhu W, Shi F, Liu Y, Li J, Qin W, Li K, Yu C, Jiang T (2009) Thick visual cortex in the early blind. J Neurosci 29(7): 2205-2211.

Jones DK, Knosche TR, Turner R (2013) White matter integrity, fiber count, and other fallacies: the do's and don'ts of diffusion MRI. Neuroimage 73: 239-254.

Kaule FR, Wolynski B, Gottlob I, Stadler J, Speck O, Kanowski M, Meltendorf S, Behrens-Baumann W, Hoffmann MB (2014) Impact of chiasma opticum

malformations on the organization of the human ventral visual cortex. Hum Brain Mapp 35(10): 5093-5105.

Kim HJ, Im K, Kwon H, Lee JM, Ye BS, Kim YJ, Cho H, Choe YS, Lee KH, Kim ST, Kim JS, Lee JH, Na DL, Seo SW (2015) Effects of amyloid and small vessel disease on white matter network disruption. J Alzheimers Dis 44(3): 963-975.

Kou Z, Iraji A (2014) Imaging brain plasticity after trauma. Neural Regen Res 9(7): 693-700.

Kral A, Sharma A (2012) Developmental neuroplasticity after cochlear implantation. Trends Neurosci 35(2): 111-122.

Leistedt SJ, Coumans N, Dumont M, Lanquart JP, Stam CJ, Linkowski P (2009) Altered sleep brain functional connectivity in acutely depressed patients. Hum Brain Mapp 30(7): 2207-2219.

Li Q, Song M, Fan L, Liu Y, Jiang T (2015) Parcellation of the primary cerebral cortices based on local connectivity profiles. Front Neuroanat 9: 50.

Liao W, Zhang Z, Pan Z, Mantini D, Ding J, Duan X, Luo C, Lu G, Chen H (2010) Altered functional connectivity and small-world in mesial temporal lobe epilepsy. PLoS One 5(1): e8525.

Liepert J, Bauder H, Miltner WH, Taub E, Weiller C (2000) Treatment-induced cortical reorganization after stroke in humans. Stroke 31(6): 1210-1216.

Liu H, Li H, Wang Y, Lei X (2014) Enhanced brain small-worldness after sleep deprivation: a compensatory effect. J Sleep Res 23(5): 554-563.

Lynall ME, Bassett DS, Kerwin R, McKenna PJ, Kitzbichler M, Muller U, Bullmore E (2010) Functional connectivity and brain networks in schizophrenia. J Neurosci 30(28): 9477-9487.

Mccarthy P, Benuskova L, Franz EA (2014) The age-related posterior-anterior shift as revealed by voxelwise analysis of functional brain networks. Frontiers in Aging Neuroscience 6.

Menon V (2011) Large-scale brain networks and psychopathology: a unifying triple network model. Trends Cogn Sci 15(10): 483-506.

Mohammad S, Gottlob I, Kumar A, Thomas M, Degg C, Sheth V, Proudlock FA (2011) The functional significance of foveal abnormalities in albinism measured using spectral-domain optical coherence tomography. Ophthalmology 118(8): 1645-1652.

Mohammad S, Gottlob I, Sheth V, Pilat A, Lee H, Pollheimer E, Proudlock FA (2015) Characterization of Abnormal Optic Nerve Head Morphology in Albinism Using Optical Coherence Tomography. Invest Ophthalmol Vis Sci 56(8): 4611-4618.

Morland A, Hoffmann M, Neveu M, Holder G (2002) Abnormal visual projection in a human albino studied with functional magnetic resonance imaging and visual evoked potentials. Journal of Neurology, Neurosurgery & Psychiatry 72(4): 523-526.

Nakamura T, Hillary FG, Biswal BB (2009) Resting network plasticity following brain injury. PLoS One 4(12): e8220.

Newman ME (2002) Assortative mixing in networks. Physical review letters 89(20): 208701.

Newman ME (2006) Modularity and community structure in networks. Proceedings of the National Academy of Sciences 103(23): 8577-8582.

Odom JV, Bach M, Brigell M, Holder GE, McCulloch DL, Tormene AP, Vaegan (2010) ISCEV standard for clinical visual evoked potentials (2009 update). Doc Ophthalmol 120(1): 111-119.

Owen JP, Ziv E, Bukshpun P, Pojman N, Wakahiro M, Berman JI, Roberts TP, Friedman EJ, Sherr EH, Mukherjee P (2013) Test-retest reliability of computational network measurements derived from the structural connectome of the human brain. Brain Connect 3(2): 160-176.

Park H-J, Friston K (2013) Structural and functional brain networks: from connections to cognition. Science 342(6158): 1238411.

Raemaekers M, Schellekens W, van Wezel RJ, Petridou N, Kristo G, Ramsey NF (2014) Patterns of resting state connectivity in human primary visual cortical areas: a 7T fMRI study. Neuroimage 84: 911-921.

Rocca MA, Valsasina P, Meani A, Falini A, Comi G, Filippi M (2014) Impaired functional integration in multiple sclerosis: a graph theory study. Brain Struct Funct (in press).

Rubinov M, Sporns O (2010a) Complex network measures of brain connectivity: uses and interpretations. Neuroimage 52(3): 1059-1069.

Rubinov M, Sporns O (2010b) Complex network measures of brain connectivity: uses and interpretations. Neuroimage 52(3): 1059-1069.

Rudie JD, Brown J, Beck-Pancer D, Hernandez L, Dennis E, Thompson P, Bookheimer S, Dapretto M (2013) Altered functional and structural brain network organization in autism. NeuroImage: clinical 2: 79-94.

Schmitz B, Käsmann-Kellner B, Schäfer T, Krick CM, Grön G, Backens M, Reith W (2004) Monocular visual activation patterns in albinism as revealed by functional magnetic resonance imaging. Human brain mapping 23(1): 40-52.

Schmitz B, Schaefer T, Krick CM, Reith W, Backens M, Kasmann-Kellner B (2003) Configuration of the optic chiasm in humans with albinism as revealed by magnetic resonance imaging. Invest Ophthalmol Vis Sci 44(1): 16-21.

Sheth V, Gottlob I, Mohammad S, McLean RJ, Maconachie GD, Kumar A, Degg C, Proudlock FA (2013) Diagnostic potential of iris cross-sectional imaging in albinism using optical coherence tomography. Ophthalmology 120(10): 2082-2090.

Sidaros A, Engberg AW, Sidaros K, Liptrot MG, Herning M, Petersen P, Paulson OB, Jernigan TL, Rostrup E (2008) Diffusion tensor imaging during recovery from severe traumatic brain injury and relation to clinical outcome: a longitudinal study. Brain 131(Pt 2): 559-572.

Soltesz I, Staley K (2011) Computational neuroscience in epilepsy. Waltham, MA: Academic Press.

Striem-Amit E, Ovadia-Caro S, Caramazza A, Margulies DS, Villringer A, Amedi A (2015) Functional connectivity of visual cortex in the blind follows retinotopic organization principles. Brain 138(Pt 6): 1679-1695.

von dem Hagen EA, Hoffmann MB, Morland AB (2008) Identifying human albinism: a comparison of VEP and fMRI. Investigative ophthalmology & visual science 49(1): 238-249.

von dem Hagen EA, Houston GC, Hoffmann MB, Jeffery G, Morland AB (2005) Retinal abnormalities in human albinism translate into a reduction of grey matter in the occipital cortex. Eur J Neurosci 22(10): 2475-2480.

Von Dem Hagen EA, Houston GC, Hoffmann MB, Morland AB (2007) Pigmentation predicts the shift in the line of decussation in humans with albinism. European Journal of Neuroscience 25(2): 503-511.

Wandell BA (1995) Foundations of vision. Sunderland, MA: Sinauer Associates.

Wandell BA, Dumoulin SO, Brewer AA (2007) Visual field maps in human cortex. Neuron 56(2): 366-383.

Wang J, Wyatt LM, Felius J, Stager DR, Stager DR, Birch EE, Bedell HE (2010a) Onset and Progression of With-the-Rule Astigmatism in Children with Infantile Nystagmus Syndrome. Investigative Ophthalmology & Visual Science 51(1): 594-601.

Wang J, Zuo X, He Y (2010b) Graph-based network analysis of resting-state functional MRI. Front Syst Neurosci 4: 16.

Wang L, Zhu C, He Y, Zang Y, Cao Q, Zhang H, Zhong Q, Wang Y (2009) Altered small-world brain functional networks in children with attention-deficit/hyperactivity disorder. Hum Brain Mapp 30(2): 638-649.

Watts DJ, Strogatz SH (1998) Collective dynamics of 'small-world'networks. Nature 393(6684): 440-442.

Welton T, Kent DA, Auer DP, Dineen RA (2014) Reproducibility of Graph-Theoretic Brain Network Metrics: A Systematic Review. Brain Connect 5(4): 193-202.

Wolynski B, Kanowski M, Meltendorf S, Behrens-Baumann W, Hoffmann MB (2010) Self-organisation in the human visual system--visuo-motor processing with congenitally abnormal V1 input. Neuropsychologia 48(13): 3834-3845.

Yu L, Yin X, Dai C, Liang M, Wei L, Li C, Zhang J, Xie B, Wang J (2014) Morphologic changes in the anterior and posterior subregions of V1 and V2 and the V5/MT+ in patients with primary open-angle glaucoma. Brain Res 1588: 135-143.

Zhong Z, Zhao T, Luo J, Guo Z, Guo M, Li P, Sun J, He Y, Li Z (2014) Abnormal topological organization in white matter structural networks revealed by diffusion tensor tractography in unmedicated patients with obsessive-compulsive disorder. Prog Neuropsychopharmacol Biol Psychiatry 51: 39-50.

Figure and Table Legends

Figure 1. Summary of the Graph-Theoretic Analysis.

The first step shows an example weighted association matrix, in which each row and column represents a brain region. Each coloured dot represents the Pearson correlation coefficient for the two fMRI timeseries extracted from the corresponding regions. The smaller horizontal line in the matrix shows pairs of regions' interhemispheric connectivities. The data from this matrix can be represented as a graph, as in the second step. By applying a threshold, the weakest connections are removed until a desired density is reached. Over a range of densities, the value of a summary graph metric is calculated, as shown in step 3. In step 4, we calculate the area under the line to give the final metric score.

Figure 2. V1 Interhemispheric Connectivity.

(A) Boxplot showing significantly higher functional connectivity between primary visual cortices in the albinism group compared to controls, and (B) nonsignificant difference in streamline density measurements between primary visual cortices compared to controls. (C) An example showing the calcarine sulci in light blue and, in red/yellow, the probability map for streamlines passing between the two regions.

Figure 3. Brain Network Properties.

Boxplots showing (A) between-group differences in graph metrics based on functional connectivity and (B) between-group differences in graph metrics based on streamline density. Metrics for which there was a significant between-group difference are indicated with an asterisk.

Table I. V1 Interhemispheric Connectivity.

Mann-Whitney U test results for the between-group differences in functional connectivity and streamline density between primary visual cortices. The values for streamline density are corrected for ROI volume.

Table II. Functional brain network properties.

Mann-Whitney U tests for equality of medians for whole-brain network metric integrals derived from fMRI data between albinism and control groups. Values given are the ratio between the subjects' score and the score from 1000 randomly-generated networks which preserve degree sequence.

Table III. Structural brain network properties.

Mann-Whitney U tests for equality of medians for whole-brain network metrics derived from DTI data between albinism and control groups. Values given are the ratio between the subjects' score and the score from 1000 randomly-generated networks which preserve degree sequence.

Tables

Table I.

Connectivity Measure	Control Median (IQR)	Albinism Median (IQR)	U	p (two-tail)
Functional Connectivity (r) – Whole V1	0.61 (0.55-0.68)	0.74 (0.62-0.82)	164	0.012 *
Anterior	**0.73 (0.59-0.82)**	**0.75 (0.66-0.82)**	**178**	**0.030***
Posterior	**0.71 (0.64-0.79)**	**0.80 (0.77-0.89)**	**160**	**0.010***
Streamline Density – Whole V1	8.78 (2.66-28.08)	10.64 (3.30-25.15)	174	0.713
Anterior	3.60 (0.53-8.09)	4.09 (0.98-11.47)	152	0.322
Posterior	2.29 (0.28-6.39)	3.69 (0.97-7.83)	146	0.246

* p-values significant after FDR correction.

Table II.

Metric	Control Median (IQR)	Albinism Median (IQR)	U	p (two-tail)
Clustering Coefficient	0.596 (0.550-0.698)	0.700 (0.608-0.804)	107	0.005 *
Characteristic Path Length	1.242 (1.222-1.264)	1.272 (1.248-1.322)	133	0.031
Small-Worldness	0.871 (0.806-0.980)	0.985 (0.880-1.096)	105	0.004 *
Assortativity	-3.560 (-5.151--2.842)	-4.220 (-5.261--2.793)	182	0.356
Modularity	4.895 (4.882-5.209)	5.226 (4.934-5.863)	128	0.022

* p-values significant after FDR correction.

Table III.

Metric	Control Median (IQR)	Albinism Median (IQR)	U	p (two-tail)
Clustering Coefficient	0.306 (0.255-0.376)	0.290 (0.243-0.346)	111	0.522
Characteristic Path Length	1.212 (1.179-1.240)	1.205 (1.157-1.234)	117	0.376
Small-Worldness	0.330 (0.265-0.395)	0.310 (0.264-0.387)	121	0.792
Assortativity	-0.108 (-0.433-0.414)	0.037 (-0.149-0.273)	127	0.591
Modularity	3.313 (2.997-3.581)	3.312 (3.065-3.618)	134	0.784

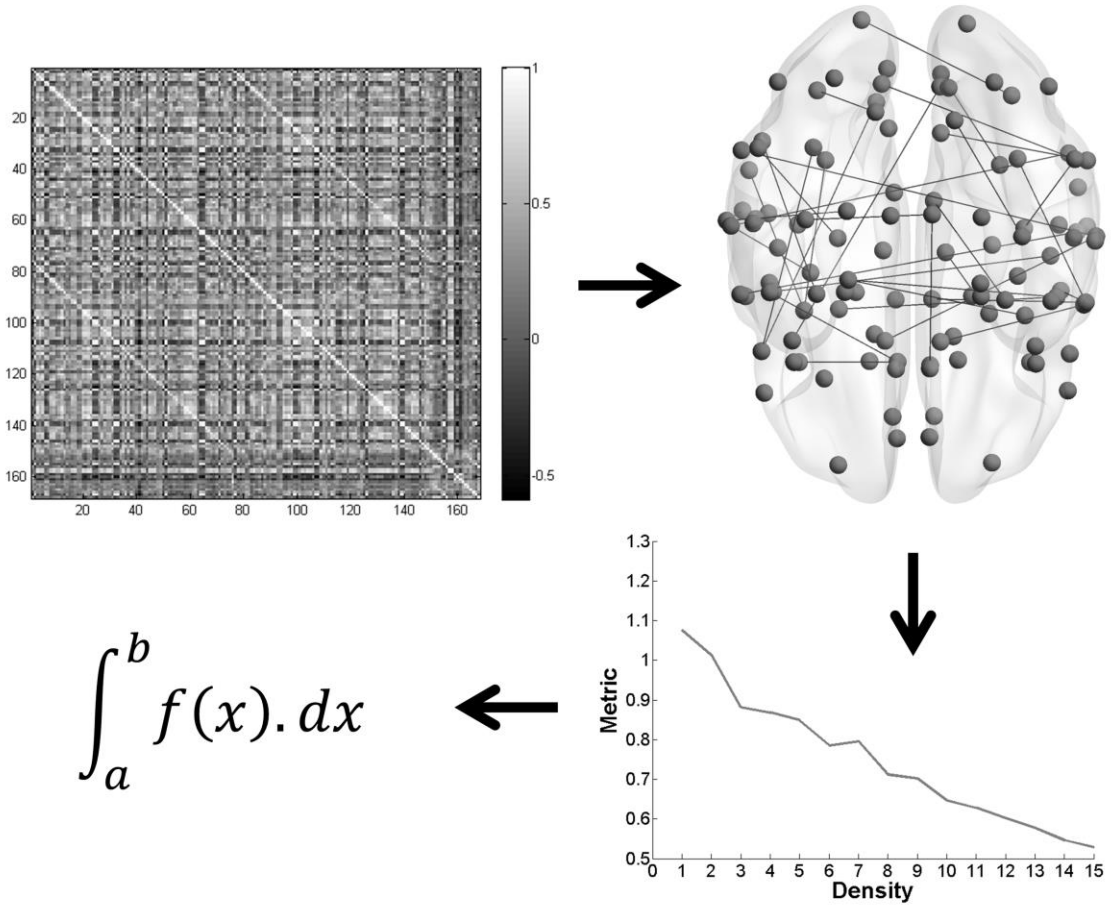
20
40
60
80
100
120
140
160
1
0.5
0
-0.5
Metric
Density
$\int_a^b f(x).dx$

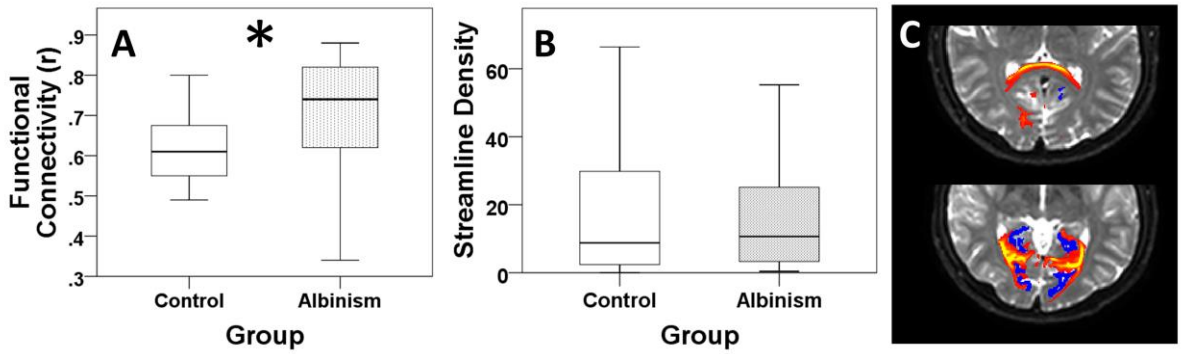
A
*
Functional Connectivity (r)
.9
.8
.7
.6
.5
.4
.3
Control
Albinism
Group
B
Streamline Density
60
40
20
0
Control
Albinism
Group
C

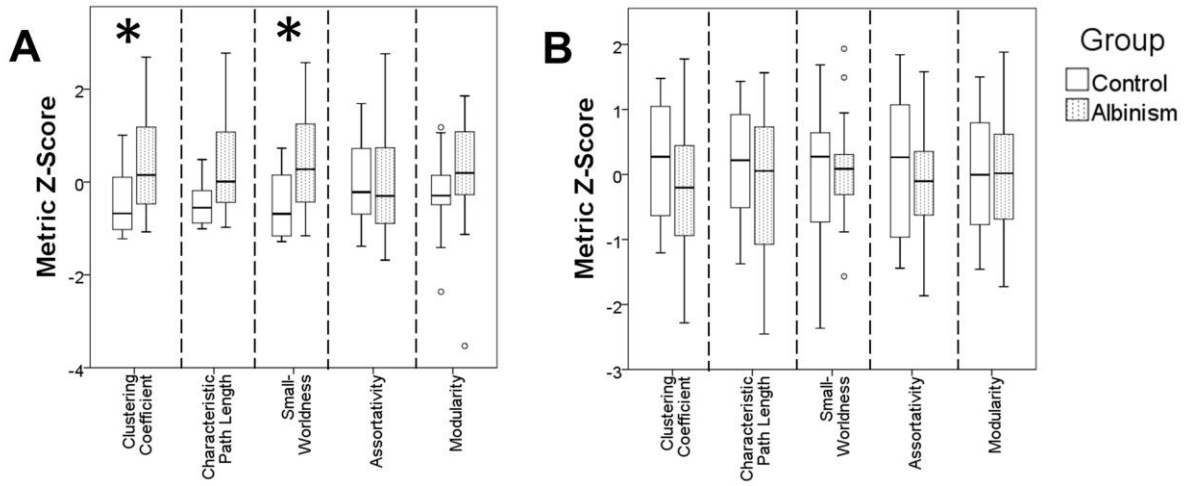
A
B
Metric Z-Score
Group
Control
Albinism
Clustering Coefficient
Characteristic Path Length
Small-Worldness
Assortativity
Modularity
*
*